THE ROLE OF DENSITY IN ACOUSTIC FULL WAVEFORM INVERSION OF MARINE REFLECTION SEISMICS

A. Przebindowska, A. Kurzmann, D. Köhn, and T. Bohlen

email: *anna.przebindowska@kit.edu*

keywords: *waveform tomography, density inversion, marine seismics*

ABSTRACT

Full waveform inversion (FWI) is a data-fitting method that exploits the full information from the seismic data to provide high-resolution models of the subsurface. To reconstruct realistic models from the field measurements the forward modeling should correctly account for wave propagation phenomena present in the recorded data. This mainly concerns the correct modeling of seismic amplitudes that are sensitive not only to the velocity variations, but also to the density, attenuation, anisotropy, source directivity effects, and to the seismic noise.

The objective of this study is to investigate the role of density in the reconstruction of reliable P-wave velocity models in the marine environment. We generated a realistic, synthetic data set for the acoustic Marmousi model with the conventional streamer geometry, and the frequency range from 3 to 20 Hz. To investigate the footprint of density on FWI we performed series of numerical experiments, testing various initial density models and different strategies for the density update. Our results suggest that it is important to include a realistic density information into the inversion scheme and that the more accurate density models bring improvement in the P-wave velocity estimation.

Moreover, we investigated the potential benefits of multi-parameter inversion (for P-wave velocity and density) of the noisy data, by considering random and spatially coherent noise. Since density is difficult to recover, a more efficient multi-parameter inversion strategy would be required to successfully compensate for the amplitude errors in the data.

INTRODUCTION

Full waveform inversion is based on minimizing the data residuals between the observed and modeled data. Choice of the objective function for inversion allows to exploit both the amplitude and phase of the observed wavefields, or to construct the phase-only (purely kinematic) or amplitude-only (dynamic) approach. Each minimization criterion shows different behavior in the inversion framework and different sensitivity to noise (Brossier et al., 2010). The least-squares norm (L2-norm), which is the most commonly used objective function (Virieux and Operto, 2009), exploits both travel-time and amplitude information to invert for the subsurface parameters. Since the amplitude of reflected seismic waves is affected by the local impedance - product of velocity and density - assuming the P-wave velocity as the only variable parameter results in incorrect modeling of seismic amplitudes. Therefore, it would be favourable to introduce additional parameters not only in the inversion of land data but also to FWI of data recorded in the marine environment.

In this study we investigate the effect of density on the reconstruction of P-wave velocity models from marine seismic data. Since the density is a difficult parameter to reconstruct (Forgues and Lambaré, 1997), in most of the case studies of real marine reflection data the authors only invert for the P-wave velocity. Density is usually estimated using an empirical formula (Hicks and Pratt, 2001; Boonyasiriwat et al., 2010; Shipp and Singh, 2002; Kelly et al., 2010; Delescluse et al., 2011) or is fixed to a constant value (Bae et al., 2010; Operto et al., 2004). Here, we consider 2D acoustic time-domain inversion of a synthetic streamer

data generated from heterogeneous P-velocity V_P and density ρ models. We run series of inversion tests assuming different initial density information and diverse stategies for density update within the inversion scheme. We use a good initial V_P model in order to highlight the density footprint on the waveform inversion. To provide a quantitative estimate of inversion results we compare the final data residuals and we measure the RMS misfit of the final velocity models.

To include both, amplitude and phase information to FWI we need to account for these wave propagation effects that are not simulated in our models. Seismic data from marine explorations are usually inverted using the 2D acoustic inversion approach (Tarantola, 1984). However, the 2D acoustic approximation does not predict elastic effects, attenuation, anisotropy, 3D effects, and seismic noise, which leads to incorrect modeling of seismic wave amplitudes. If the acoustic inversion has the P-velocity as the only unknown, then all amplitude discrepancies resulting from nonacoustic factors will be projected into the V_P model. To mitigate this problem FWI could account for additional inversion parameters, such as density or attenuation. To study the performance of the multi-parameter inversion in the presence of noise in the data we apply the V_P only and combined V_P and ρ inversion to synthetic noisy data. This test will allow to investigate whether the density inversion can partly compensate for the inversion artefacts due to the coherent or incoherent noise present in the observed data.

DENSITY MODELING AND INVERSION

The forward problem for an acoustic medium is often based on the constant density acoustic wave equation. However, the acoustic wave equation with variable density (Equation 1) would provide a better description of wave propagation in marine environments. The amplitude of acoustic waves is affected not only by the P-wave velocity but primarily by the local acoustic impedance, which is the product of density and velocity. A density contrast contributes to an acoustic impedance contrast, which affects the reflection coefficient. Variation in seismic reflection amplitudes depends also on the angle of incidence of seismic arrival on the reflector. This offset dependent amplitude change (AVO) contains information on both the compressional properties of rock as well as density. Thus, if we want to match both amplitude and phases in the real data inversion, we should take into account the density effect. Otherwise, the amplitude variations in observed data will be mapped into velocity models only.

The 2D variable density acoustic wave equation is defined as:

$$\frac{1}{{V_P}^2}\frac{1}{\rho}\frac{\partial^2 p}{\partial t^2} = \left[\frac{\partial}{\partial x}\left(\frac{1}{\rho}\frac{\partial p}{\partial x}\right) + \frac{\partial}{\partial z}\left(\frac{1}{\rho}\frac{\partial p}{\partial z}\right)\right] + f \ , \tag{1}$$

where $p(x,z,t)$ is the pressure field, $\rho(x,z)$ is the density, $V_P(x,z)$ is the P-wave velocity, and $f(x,z,t)$ is the source term.

Besides the reconstruction of V_P models, acoustic FWI can account for the density as well. In the waveform inversion scheme based on the general approach of Tarantola (1984) and Mora (1987) the model parameters m are updated iteratively along the conjugate gradient direction δc with the step length μ_n:

$$m_n = m_{n-1} - P\mu_n \delta c_n \tag{2}$$

where m_n is the model update at iteration n, and P the preconditioning operator. The density gradient at iteration n can be expressed by

$$\delta\rho_n(x,z) = \sum_{sources}\int_0^T dt \ \text{grad}\ p_n^{'}(x,z,t)\ \text{grad}\ p_n(x,z,t) \ , \tag{3}$$

where p_n is the forward propagated field in the current model, and $p_n^{'}$ is generated by propagating the residual data from all receiver positions backward in time.

Estimating density values from seismic data is an ill-posed inverse problem (Debski and Tarantola, 1995). The density is poorly resolved especially from the short-offset P-wave velocity, because the V_P and density radiation patterns are the same for small angles of incidence (Tarantola, 1986). The influence of the density contrast on the V_P reflection amplitude becomes visible at larger angles. Therefore, in order to resolve density information from seismic data the wide-angle recordings might be required (Roberts, 2000). But if the data are recorded over a limited range of angles of incidence and the density contrasts

are moderate it would be difficult to reconstruct accurate density models. In such a case the density inversion could be additionally constrained to control the relation between density and V_P, so that the density character follow that of P-wave velocity, or acoustic impedance I_P, depending on the choice of inversion parameters (Tarantola, 1986).

NUMERICAL EXPERIMENT SETTINGS

Modeling parameters

The numerical tests are based on the acoustic Marmousi model (Versteeg, 1994), the P-wave velocity and density models are shown in Figure 1. The model consists of layered sediments with two hydrocarbon reservoirs: a gas lense at the depth of 900 m and a thin oil sand layer at 1520 m, with an average vertical thickness of 38 and 40 m respectively. The seafloor depth is at 300 m, which means that the surface-related multiples can be clearly observed in the data.

The design of the numerical experiment aimed to reflect the real measurement conditions of marine reflection seismic (Figure 1). The source is a pressure source, located 7.5 m below the air-water interface, with the Ricker wavelet time function. Since the lack of low frequencies in seismic recordings is a general problem, we have limited the frequency content of a signal to a bandwidth from 3 to 20 Hz. The acquisition setup mimics the conventional single-component streamer survey. The streamer consists of 160 hydrophones with a spacing of 25 m located at 7.5 m depth.

Observed data

The synthetic noise-free data were calculated using the finite-difference solution of 2D acoustic wave equation. The total of 50 shot gathers were generated at a 50 m interval with 3 seconds of data. This data set is used in the first part of inversion tests.

To investigate the potential benefits of joint P-velocity and density inversion in the presence of noise we generated two sets of data affected by the incoherent and coherent noise pattern. In the first case the original noise-free data were contaminated with a random 20 percent band-limited Gaussian noise (Figure 2). The second data set was created by superimposing spatially coherent noise generated from a model constisting of a diffractor in P-wave velocity embedded in a homogeneous fullspace, with a background velocity of 1500 m/s (Figure 3). Such a coherent noise that cannot be predicted by the 2D acoustic model may represent elastic effects (converted waves) or 3D reflection phenomena.

Inversion process

To find an optimum model we search for the global minimum of the misfit function defined as the L2-norm of the data residuals. However, one of the major problems in the waveform tomography is related to the nonlinearity of the objective function. In some cases the high complexity of the seismic data or high noise level might cause a very complex error function and, in consequence, the algorithm can get stuck easily in a local minimum. To mitigate this problem we follow the multi-scale approach proposed by Bunks et al. (1995). The nonlinearity of the objective function is frequency dependent, i.e. the misfit function is more linear at low frequencies, whereas a lot of local minima are present at higher frequencies. Therefore, the inversion starts at low frequencies and the higher frequency content is gradually added. Furthermore, to correct for the amplitude loss with depth due to geometrical spreading and to enhance deeper parts of the model, the linear gradient scaling with depth is implemented.

The starting V_P model is a 1D smooth representation of the true velocity distribution. The water bottom parameters are not explained correctly by the starting P-wave model. To allow for a direct comparison of the results, the same inversion scheme and the initial V_P model were used in all experiments. The update of water bottom parameters (V_P, density, depth) is allowed.

Results analysis

In order to quantitatively assess the inversion results we measure initial and final errors, both in the data and in the model. Since the waveform inversion is an ill-posed and non-unique problem this will help to

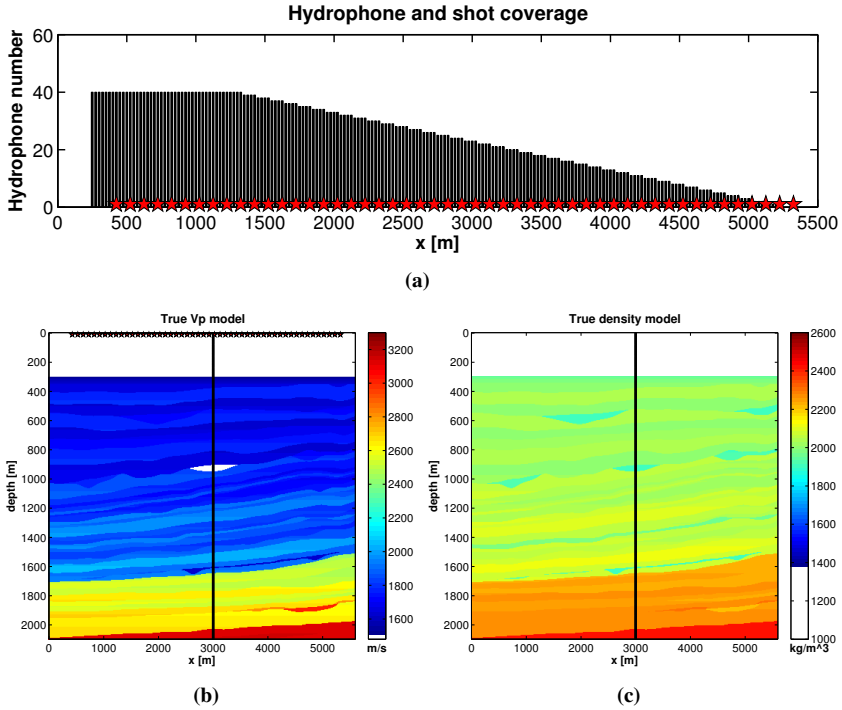

Figure 1: (a) The acquisition geometry of the numerical experiment, with the receiver fold. Synthetic true models for (b) P-wave velocity and (c) density.

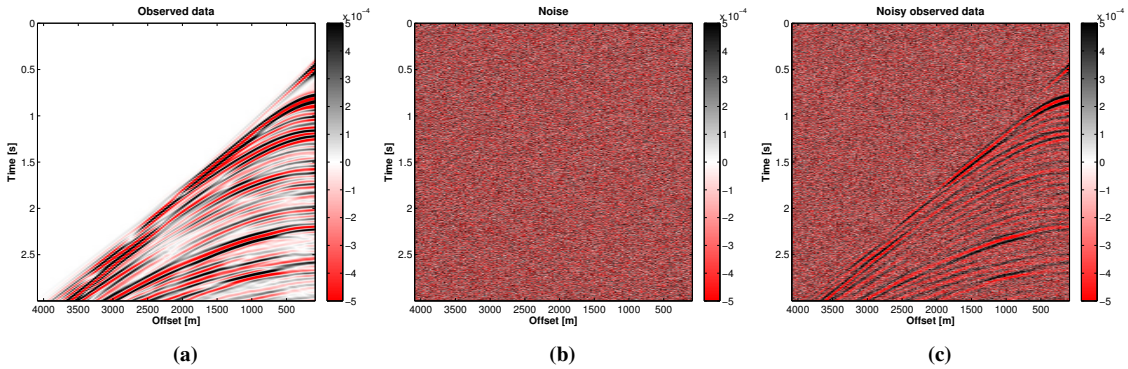

Figure 2: Synthetic pressure data, shot 50. (a) Noise-free, (b) random Gaussian noise, (c) noisy data.

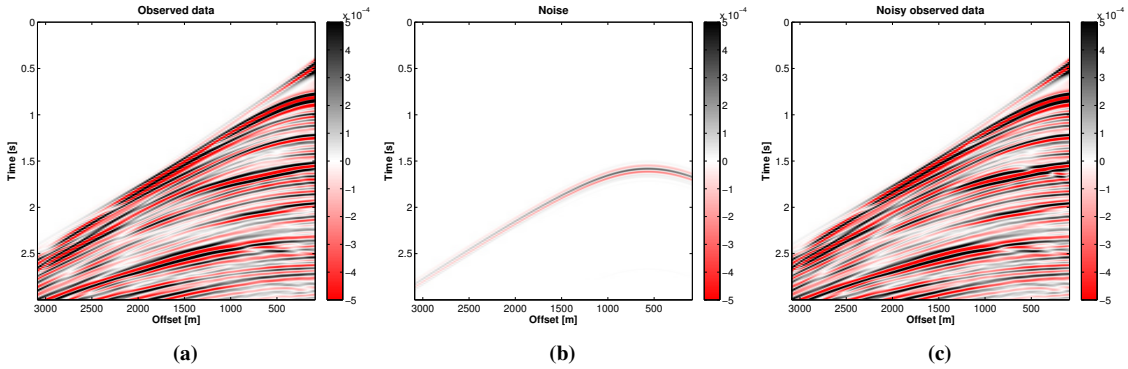

Figure 3: Synthetic pressure data, shot 30. (a) Noise-free, (b) spatially coherent noise, (c) noisy data.

determine whether the reduction of residuals is followed by a better estimation of model parameters.

The difference between modeled, p, and observed data, p^{obs}, is measured by the least-squares error and is expressed in terms of the percentage of the observed data energy E_{obs}:

$$L2_{relative} = \frac{L2_{residuals}}{E_{obs}} = \frac{\frac{1}{2}(p - p^{obs})^2}{\frac{1}{2}(p^{obs})^2} \cdot 100\% \ , \tag{4}$$

To assess the quality of the final velocity models we measure the normalized RMS error between the real and reconstructed P-velocities within the area of the model update:

$$V_{Perror} = \sqrt{\frac{\sum_{i=1}^{n} (\hat{V_{Pi}} - V_{Pi})^2}{\sum_{i=1}^{n} V_{Pi}^2}} \ , \tag{5}$$

where $\hat{V_{Pi}}$ is the estimated P-wave velocity for the ith grid point, and V_{Pi} is the true velocity value.

INVERSION RESULTS

Noise-free data

In this section we apply acoustic waveform inversion to noise-free data to investigate the effect of density on P-wave models reconstruction. Moreover, we want to find the most efficient strategy for including density information into the inversion scheme.

Figure 5c shows the part of the waveform that corresponds to the reflection of seismic energy at density contrasts. The amplitude of the primary and multiple water bottom reflections is mainly related to the strong density contrast between the water and marine sediments. The reflection coefficient of the reflectors inside the medium is influenced both by the P-wave and density contrasts.

In order to characterize the sensitivity of the waveform to density changes, we used a range of starting density models and then calculated values of the objective function (Figure 4). The reference starting density is a 1D smoothed true density model, which was varied by adding $\pm$ 25 % density perturbations along the entire profile, disregarding the water layer. The initial L2-norms computed for these starting density models vary from 53 % to 64 % of the observed data energy. The lowest misfit value corresponds to the density model, which together with the initial V_P model, gives the closest match to the real amplitude of the primary and secondary seafloor reflections, which are the most energetic events in the initial data.

For the acoustic inversion four different starting rho models were considered:

- true density model;
- in sediments: density model linked with the starting V_P model using Gardner's relationship, in water: density equals 1000 kg/m3;
- in sediments: density model linked with the starting V_P model using Brocher's relationship, in water: density equals 1000 kg/m3;
- homogeneous density model.

Gardner's $V_P - \rho$ relationship (Gardner et al., 1974) is an approximate average of the relations for a number of sedimentary rock types, weighted toward shales. The relation takes the following form:

$$\rho \ (\text{kg/m}^3) = 0.31 \cdot 1000 \cdot V_p^{0.25} \tag{6}$$

This relationship gives relatively good density estimates for sediment layers in our true model.

Additionally, we selected Brocher's density-velocity relationship (Brocher, 2005):

$$\rho \ (\text{g/cm}^3) = 1.6612V_p - 0.4721V_p^2 + 0.0671V_p^3 - 0.0043V_p^4 + 0.000106V_p^5 \tag{7}$$

This relation systematically underestimates density with respect to the true values and provides a poor initial density model.

Inversion test	starting density model	density model update
A	homogeneous rho	none
B	from V_P-ρ Brocher's relation	none
C	from V_P-ρ Brocher's relation	update with Brocher's relation
D	from V_P-ρ Brocher's relation	inversion
E	from V_P-ρ Gardner's relation	none
F	from V_P-ρ Gardner's relation	update with Gardner's relation
G	from V_P-ρ Gardner's relation	inversion
H	true rho	none

Table 1: Summary of inversion tests.

The choice of the relationship between V_P and density controls the amplitudes of reflections. It should be noted that these relationships are not valid in the presence of hydrocarbons.

We tested three different strategies for incorporating density information during the inversion process:

- starting density model is fixed during the inversion;
- density is updated after each iteration using one of the $V_p - \rho$ relationships;
- multi-parameter inversion for V_P and ρ.

Inversion results of noise-free data are summarized in Table 2 and Table 3.

To examine the resolution and accuracy of the inversion algorithm we performed an inversion test with the true density model (Figure 6). The reconstructed velocity model is nearly identical to the true model, the final RMS error equals 3.44 %. After 400 iterations the data misfit reached 0.01 % of the observed data energy. For comparison the maximum number of iterations for all other tests was set to 400.

The highest misfit values both in the data space (6.92 %) and in the model space (5.75 %) result from the constant density assumption. The final velocity model (Figure 7) shows strong artefacts around the seafloor and poor quality in deeper regions. Without the density information amplitude errors in modeling of the water bottom reflector are produced, which are then reflected in high amplitudes of the residual waveform and artefacts in V_P models.

If we include more realistic density models using empirical velocity-density formula, we can observe a general improvement in the recovery of the P-wave model (Figure 8), even if the density model is kept fixed during inversion. A combination of the good initial density model with the density update at each iteration step using a quite correct empirical relation, in this case the Gardner relationship, produced the best final result (apart from the experiment with the true density model). P-wave velocity model was very well recovered, with the RMS error reduced from 6.37 % to 3.8 %. Overall, the choice of the density-velocity relationship and the density update strategy (kept fixed or updated from V_P model) had no significant effects on the reconstruction of V_P parameter.

Finally, we tested a multi-parameter inversion. Figure 9 shows results obtained by inverting for V_P and density. The data misfit was reduced from initial 53.83 % to 0.86 %, whereas the final V_P model error is high – 5.11 %. This poor result is caused by the inaccurate inversion of the density. The density values are wrong and many interfaces are not correctly located. This misplacement of interfaces combined with the relatively strong density contrast produced reflections, that are not correlated with the reflections from the recovered velocity discontinuities. In the consequence, the velocity model had partly compensated for the amplitude errors due to incorrect density estimation.

Noisy data

To investigate the potential benefits of multi-parameter inversion in the presence of noise, we inverted two data sets contamined by different noise types: a random, Gaussian noise with the signal-to-noise ratio set to 5 (Figure 2c), and a spatially correlated noise with the moderate amplitude (Figure 3c).

Inversion results of noisy data are summarized in Table 4 and Table 5.

	initial L2-norm	**density update strategy**					
starting rho model		fixed		updated from V_P		inverted	
constant rho	82.06 %	6.92 %	(A)	-		-	
Brocher's relation	53.31 %	0.40 %	(B)	0.49 %	(C)	0.72 %	(D)
Gardner's relation	53.83 %	0.09 %	(E)	0.05 %	(F)	0.86 %	(G)
true rho model	48.62 %	0.01 %	(H)	-		-	

Table 2: Summary of noise-free data inversion results. Capital letters refer to inversion tests listed in Table 1. L2-norm of the initial and final residuals.

	initial V_P error	**density update strategy**					
starting rho model		fixed		updated from V_P		inverted	
constant rho	6.37 %	5.75 %	(A)	-		-	
Brocher's relation	6.37 %	4.28 %	(B)	4.13 %	(C)	4.99 %	(D)
Gardner's relation	6.37 %	4.02 %	(E)	3.80 %	(F)	5.11 %	(G)
true rho model	6.37 %	3.44 %	(H)	-		-	

Table 3: Summary of noise-free data inversion results. RMS error of the initial and reconstructed velocity models.

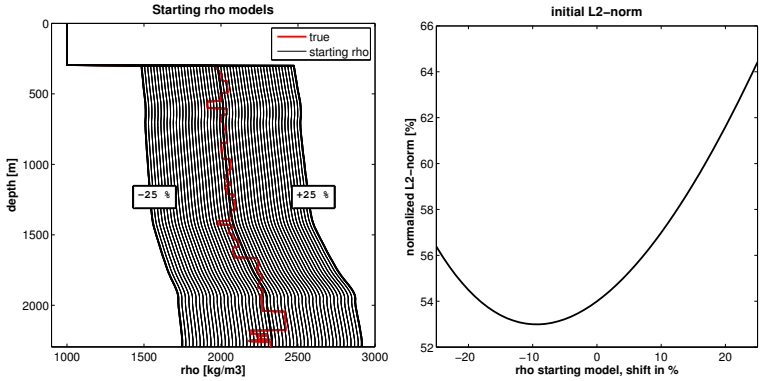

(a) **(b)**

Figure 4: (a) Set of starting density models generated by adding $\pm$ 25 % density perturbations with a 1 percent shift to the smoothed 1D true rho model. (b) Initial, normalized L2-norm that corresponds to selected starting density models.

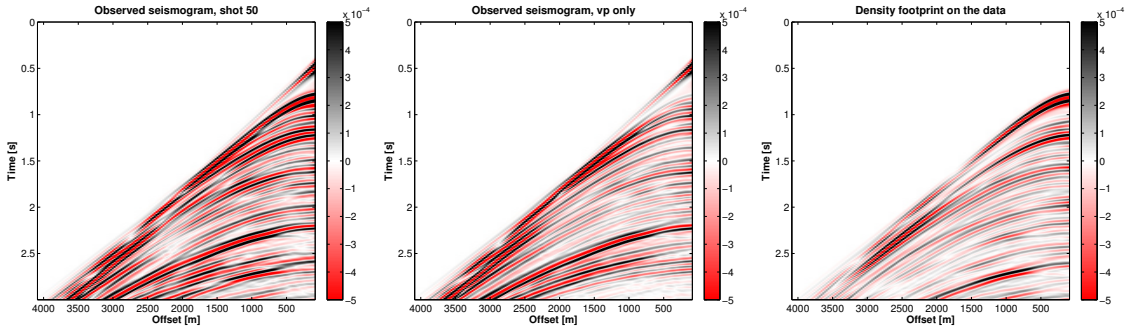

(a) **(b)** **(c)**

Figure 5: (a) Acoustic data for V_P and density model, (b) simulation for V_P model only (constant density acoustic wave modeling), (c) the difference between (a) and (b).

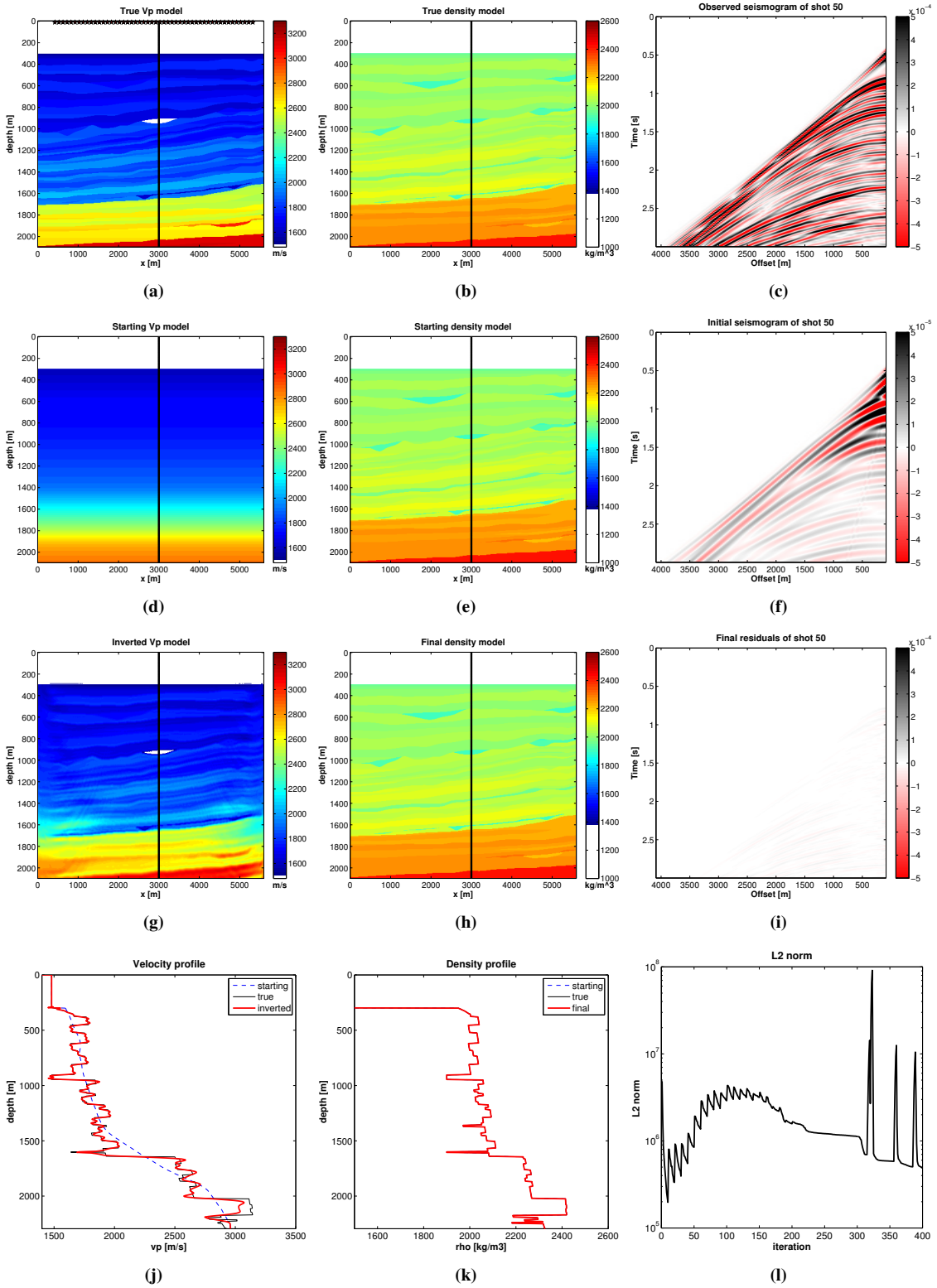

Figure 6: Inversion results for Test H. Starting rho model: true rho model; no rho model update. (a) True V_P model [m/s], (b) true rho model [kg/m3], (c) observed data for shot 50 located at x = 5325 m, (d) initial V_P model, (e) initial rho model, (f) initial synthytetics for shot 50, (g) inverted V_P model, (h) final rho model, (i) final residuals for shot 50, (j) V_P profiles, (k) rho profiles, (l) L2-norm.

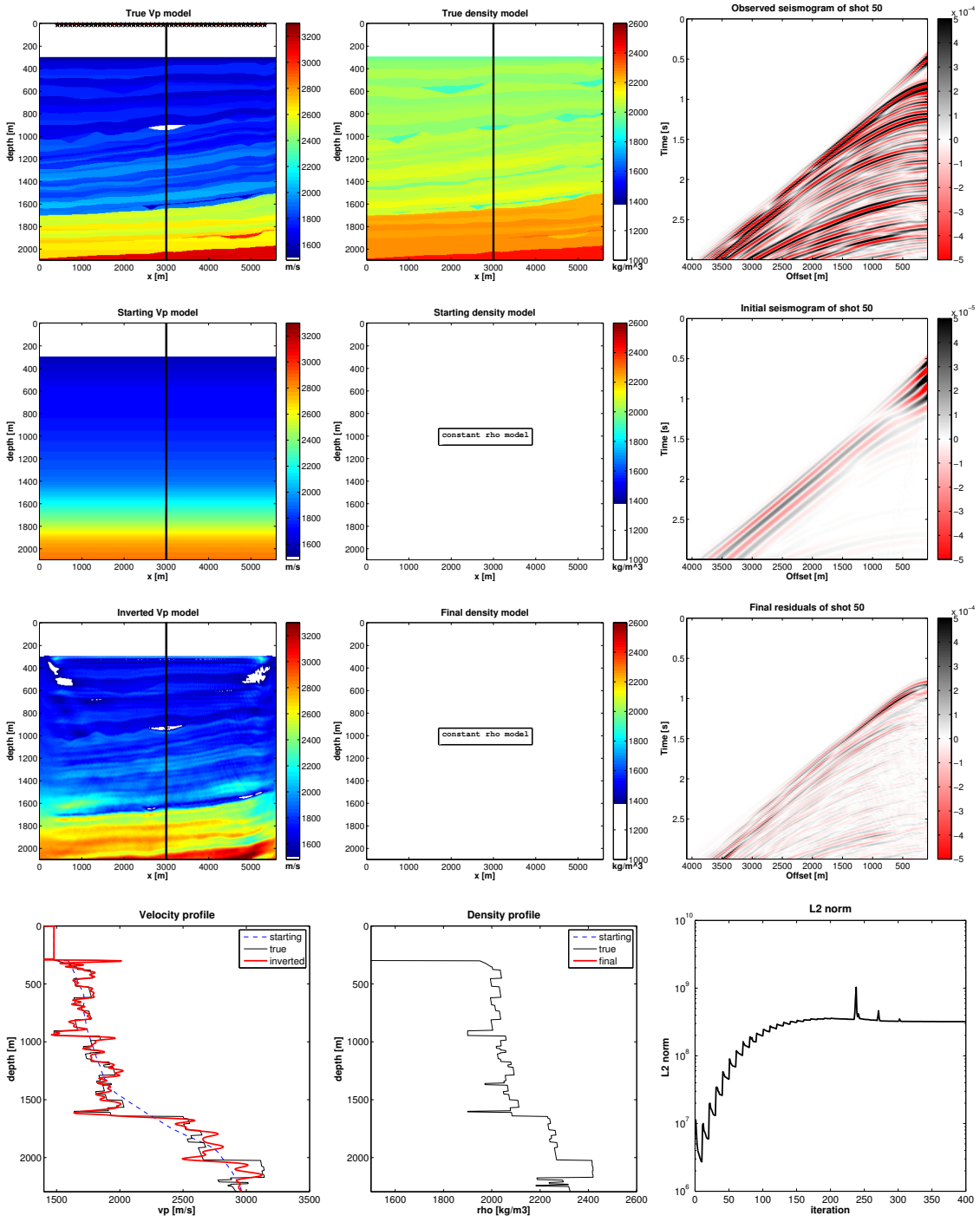

Figure 7: Inversion results for Test A. Homogeneous density model is used. For details see caption of Figure 6.

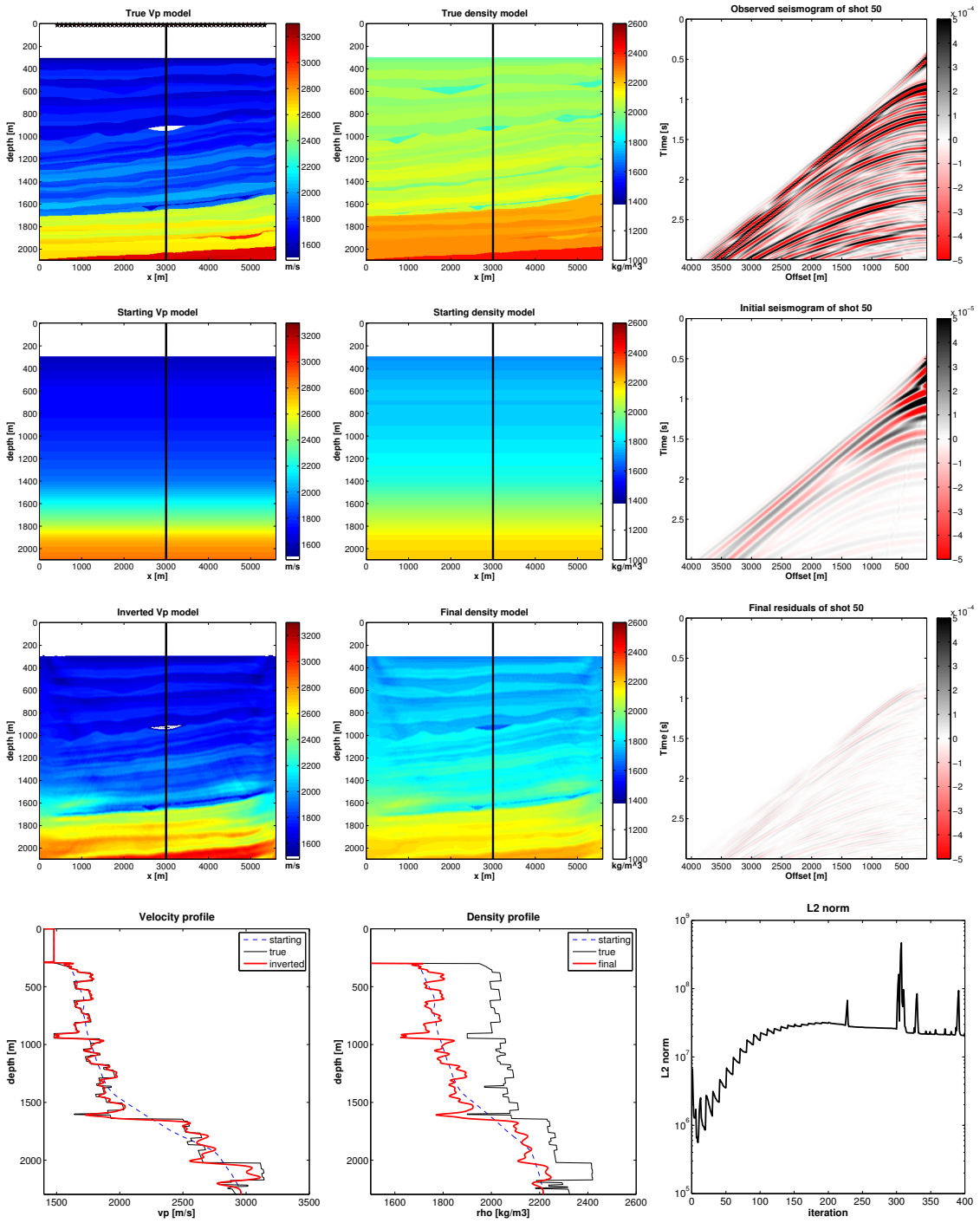

Figure 8: Inversion results for Test B. Starting rho model: computed from the starting V_P model using Brocher's relationship; rho model is updated after each iteration from the inverted V_P using Brocher's relationship. For details see caption of Figure 6.

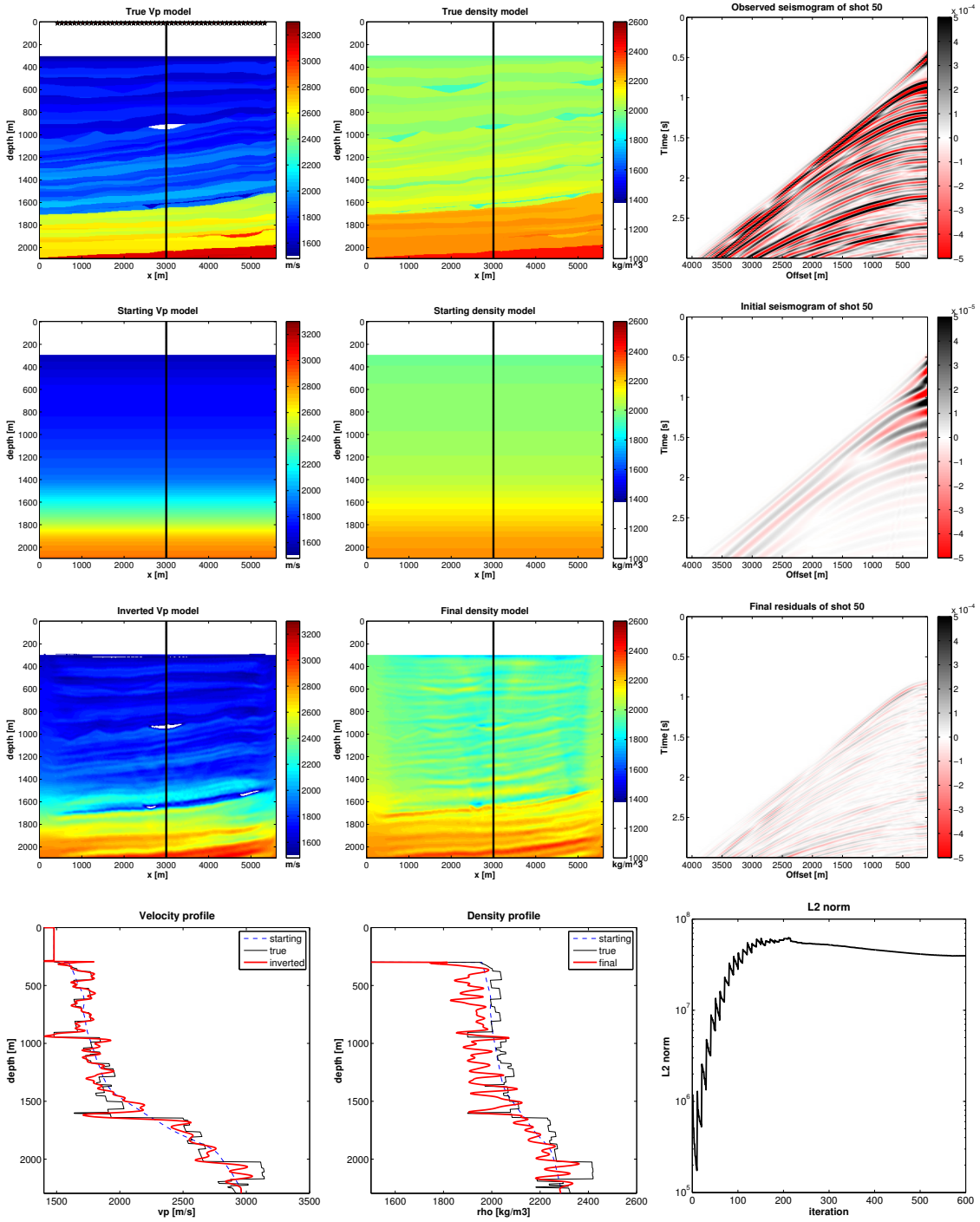

Figure 9: Inversion results for Test F. Starting rho model: computed from the starting V_P model using Gardner's relationship; multi-parameter inversion for V_P and rho. For details see caption of Figure 6.

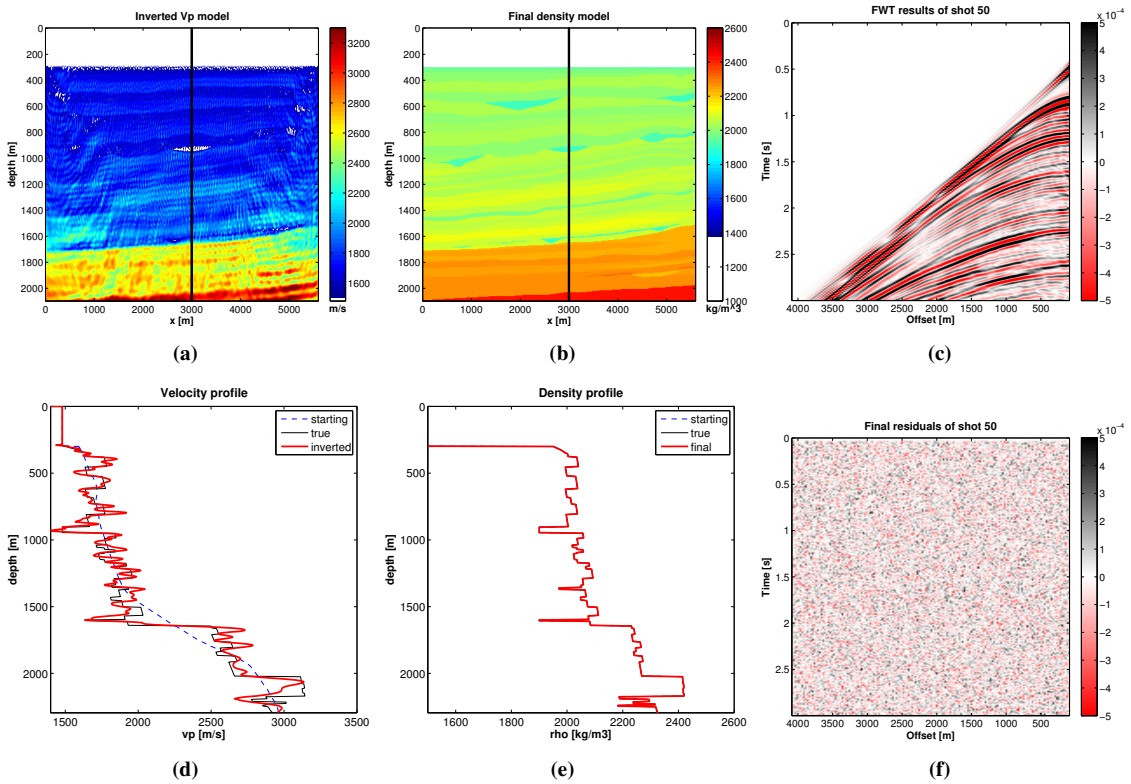

Figure 10: Inversion results of noisy data (random, Gaussian noise). Inversion for V_P only. (a) inverted V_P, (b) final rho, (c) final modeled data (shot 50), (d) V_P profiles, (e) rho profiles, (f) final residuals.

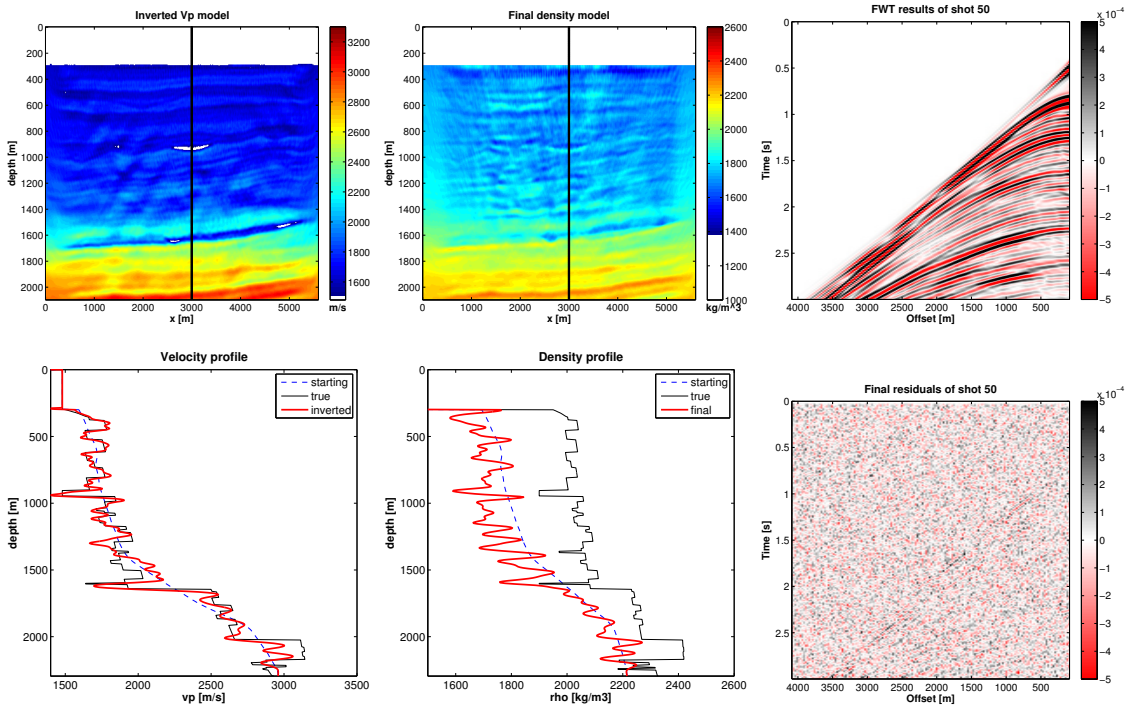

Figure 11: Inversion results of noisy data (random, Gaussian noise). Multi-parameter inversion for V_P and rho. For details see caption of Figure 10.

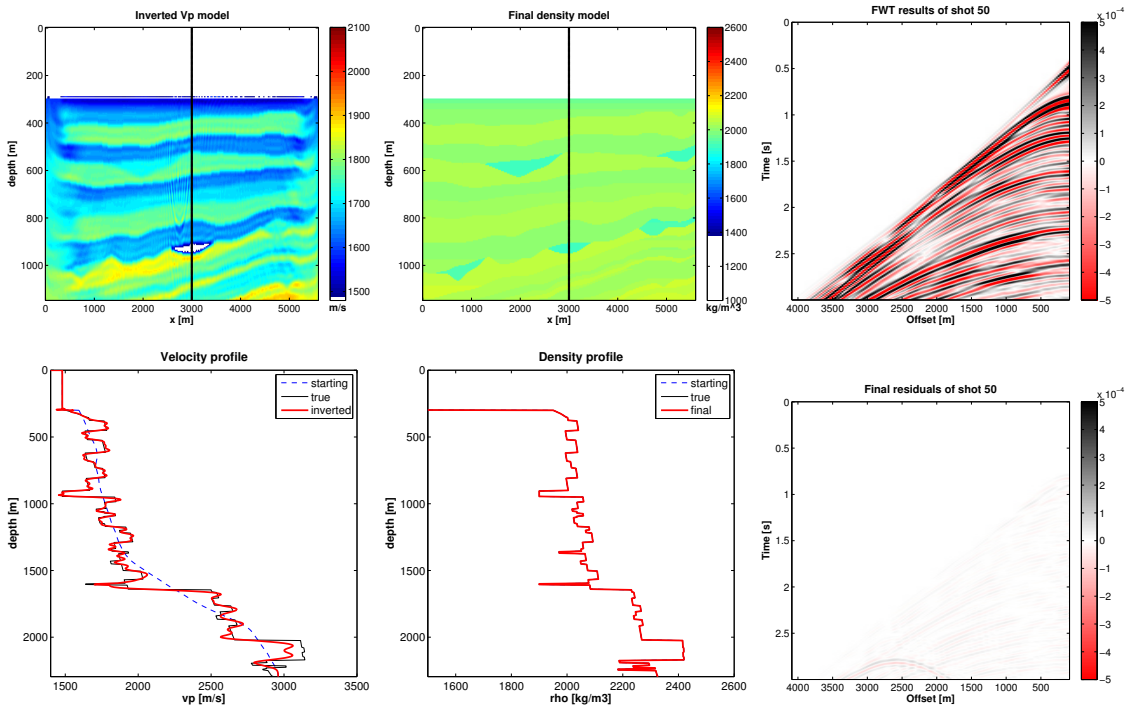

Figure 12: Inversion results of noisy data with spatially coherent noise added. Inversion for V_P only. Final models show only the shallow structures up to depth of 1200 m. For details see caption of Figure 10.

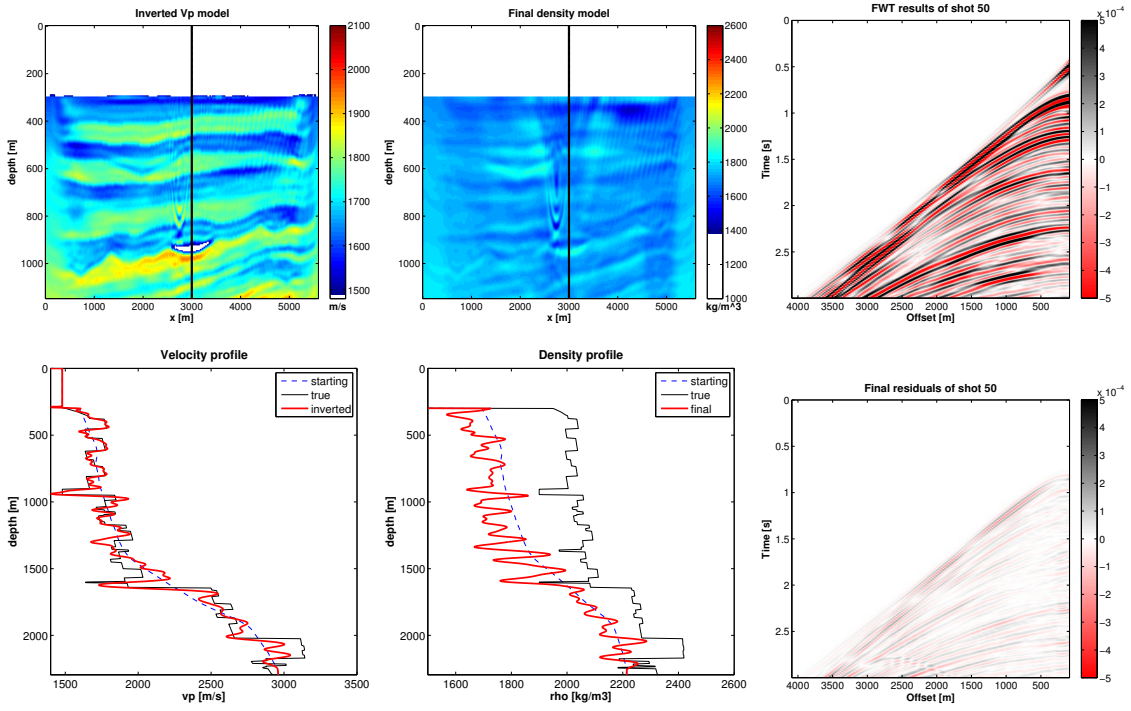

Figure 13: Inversion results of noisy data with spatially coherent noise added. Multi-parameter inversion for V_P and rho. Final models show only the shallow structures up to depth of 1200 m. For details see caption of Figure 10.

Data	Inversion parameters	Initial L2-norm	Final L2-norm
random noise	V_P	91.07 %	2.67 %
	V_P and rho	91.07 %	2.81 %
coherent noise	V_P	48.77 %	0.25 %
	V_P and rho	48.77 %	1.27 %

Table 4: Summary of noisy data inversion results. L2-norm of the initial and final residuals.

Data	Inversion parameters	Initial V_P error	Final V_P error
random noise	V_P	6.37 %	5.27 %
	V_P and rho	6.37 %	5.30 %
coherent noise	V_P	6.37 %	3.56 %
	V_P and rho	6.37 %	5.26 %

Table 5: Summary of noisy data inversion results. RMS error of the initial and reconstructed velocity models.

In the first experiment we inverted data with the random noise. Figure 10 shows the V_P only inversion results. In this case the true density model was used. Adding noise to the data produced a lot of small-scale artefacts in the final velocity image. This is a general behavior of the L2-norm, that is known to be sensitive to amplitude errors in the data and tries to explain it by introducing false structures into the models (Crase et al., 1990). The multi-parameter inversion (Figure 11) shows a much smoother reconstructed V_P model. The density "absorbed" some artefacts, nevertheless the accuracy of the recovered velocity model is low. The RMS error in the V_P model was reduced from the initial 6.37% to 5.30% after 400 iterations.

In the next experiment we inverted data affected by the spatially correlated noise. Figure 12 shows results for the V_P only inversion and Figure 13 for the multi-parameter V_P and ρ inversion. Even though the data residuals are not dominated by noise, there is a problem with focusing the energy of this event what can be seen as a smile-like effect in the reconstructed models.

The multi-parameter inversion brought no improvement in the V_P model reconstruction from the noisy data, but this is due to the problem that the density was not correctly estimated through waveform inversion even from the noise-free data.

CONCLUSIONS

In this study we applied 2D acoustic time-domain FWI to a realistic synthetic data set, which mimics the conventional marine-streamer acquisition. The very low frequencies (< 3 Hz) were removed from the data. The model used to generate synthetic data is an acoustic medium with the heterogeneous density distribution. The primary goal of this work was to investigate the role of density on the recovery of velocity models.

Our results show that the realistic density information should be directly included in the inversion process to improve the accuracy of the velocity reconstruction. This is particularly important if the least-squares objective function is used in the FWI, because this norm takes into account both amplitude and phase information of the data. Using a constant density assumption produces artefacts in the recovered velocity models, because then all reflections are interpreted in terms of velocity contrasts only.

The more accurate density models bring improvement in the V_P estimation. Therefore, it would be preferable to allow for the density inversion, rather than use a fixed relationship between velocity and density. Especially, when we take into account the fact that all empirical relations are valid only for certain types of rocks. However, the reliable estimation of density is difficult, also in our synthetic noise-free experiment. Incorrect density values combined with the misplacement of reflectors result in incorrect velocity images. Apparently, velocity compensates the amplitude errors in the modeled data produced by strong density contrasts.

To enable a successful multi-parameter inversion for P-wave velocity and density it would be necessary

to constrain the density model update. As it was mentioned by Amundsen and Ursin (1991) velocity shows faster convergence than density, mainly because the information on velocity structure is enclosed in the arrival times of seismic reflections, whereas the density is contained in the amplitude information. Therefore, the overall velocity trend should be correct before fitting the amplitudes to recover the density model.

Further work is required to investigate the best strategies for the multi-parameter inversion with the emphasis on the constrained density inversion.

ACKNOWLEDGMENTS

This work was kindly supported by the sponsors of the *Wave Inversion Technology (WIT) Consortium*, Karlsruhe, Germany. The calculations were performed on the JUROPA cluster at Jülich supercomputing center.

REFERENCES

Amundsen, L. and Ursin, B. (1991). Frequency-wavenumber inversion of acoustic data. *Geophysics*, 56(7):1027–1039.

Bae, H., Shin, C., Cha, Y., and Choi, Y. (2010). 2D acoustic – elastic coupled waveform inversion in the laplace domain. *Geophysical Prospecting*, 58:997–1010.

Boonyasiriwat, C., Schuster, G., Valasek, P., and Cao, W. (2010). Applications of multiscale waveform inversion to marine data using a flooding technique and dynamic early-arrival windows. *Geophysics*, 75(6):R129–R136.

Brocher, T. M. (2005). Empirical relations between elastic wavespeeds and density in the Earth's crust. *Bull. Seism. Soc. Am.*, 95:2081–2092.

Brossier, R., Operto, S., and Virieux, J. (2010). Which data residual norm for robust elastic frequency-domain full waveform inversion? *Geophysics*, 75(3):R37–R46.

Bunks, C., Saleck, F., Zaleski, S., and Chavent, G. (1995). Multiscale seismic waveform inversion. *Geophysics*, 60(5):1457–1473.

Crase, E., Pica, A., Noble, M., McDonald, J., and Tarantola, A. (1990). Robust elastic nonlinear waveform inversion: Application to real data. *Geophysics*, 55:527–538.

Debski, W. and Tarantola, A. (1995). Information on elastic parameteres obtained from the amplitudes of reflected waves. *Geophysics*, 60(5):1426–1436.

Delescluse, M., Nedimović, M., and Louden, K. (2011). 2d waveform tomography applied to long-streamer mcs data from the scotian slope. *Geophysics*, 76:B151–B163.

Forgues, E. and Lambaré, G. (1997). Parameterization study for acoustic and elastic ray + born inversion. *Journal of Seismic Exploration*, 6:253–278.

Gardner, G., Gardner, L., and Gregory, A. (1974). Formation velocity and density—the diagnostic basics for stratigraphic traps. *Geophysics*, 39:770–780.

Hicks, G. and Pratt, G. (2001). Reflection waveform inversion using local descent methods: Estimating attenuation and velocity over a gas-sand deposit. *Geophysics*, 66(2):598–612.

Kelly, S., Ramos-Martinez, J., Tsimelzon, B., and Crawley, S. (2010). Application of an impedance-based full-waveform inversion method for dual-sensor, single-streamer field recordings. *72nd Conference and Technical Exhibition, EAGE, Extended Abstracts*, A020.

Mora, P. (1987). Non-linear two-dimensional elastic inversion of multi-offset seismic data. *Geophysics*, 52:1211–1228.

Operto, S., Ravaut, C., Improta, L., Virieux, J., Herrero, A., and Dell'Aversana, P. (2004). Quantitative imaging of complex structures from dense wide-aperture seismic data by multiscale traveltime and waveform inversions: a case study. *Geophysical Prospecting*, 52:625–651.

Roberts, G. (2000). Wide-angle avo. *70th Ann. Internat. Mtg. Soc. Expl. Geophys., Expanded Abstracts*, AVO 2.2.

Shipp, R. and Singh, S. (2002). Two-dimensional full wavefield inversion of wide-aperture marine seismic streamer data. *Geophys. J. Int.*, 151:325–344.

Tarantola, A. (1984). Inversion of seismic reflection data in the acoustic approximation. *Geophysics*, 49:1259–1266.

Tarantola, A. (1986). A strategy for nonlinear elastic inversion of seismic reflection data. *Geophysics*, 51:1893–1903.

Versteeg, R. (1994). The marmousi experience: Velocity model determination on a synthetic complex data set. *The Leading Edge*, 13:927–936.

Virieux, J. and Operto, S. (2009). An overview of full-waveform inversion in exploration geophysics. *Geophysics*, 74(6):WCC127–WCC152.